Chapter 3 Simulation (1) – Optimization of C-aperture

In order to demonstrate the performance of the fiber-based light delivery modules, simulation was carried out in the first place as a guide to fabrication. This chapter focuses on the optimization of the C-aperture dimensions and the surface corrugation will be discussed in next chapter.

3.1 Simulation Description

3.1.1 Optical Models

The two kinds of optical models are depicted once again in Fig. 3.1-1. Light emitted from a laser diode, coupled into the single mode fiber and focused by the coreless fiber is assumed to be X-polarized with wavelength of 633 nm. For the freestanding case, the field distribution out of the coreless fiber is supposed as Gaussian distribution, inferring the wavefront is planar at the focal plane where the beam waist forms; moreover, this focused spot size is ~ 2μm which much larger than the aperture area so that the incident light can be considered as a plane wave normally into the aperture.

For the integrated case, the above-mentioned assumption also stands because the beam size is also much larger than the aperture area. The difference of the integrated case from the freestanding one is the reduced wavelength of ~430 nm due to the mean refractive index of the GRIN fiber of 1.475.

In addition, the metal film is silver with dielectric constant of -18.5-2.33*i*, which implies the skin depth of 25 nm and the film thickness is 200 nm of these two cases in order to prevent the light from leaking accordingly.

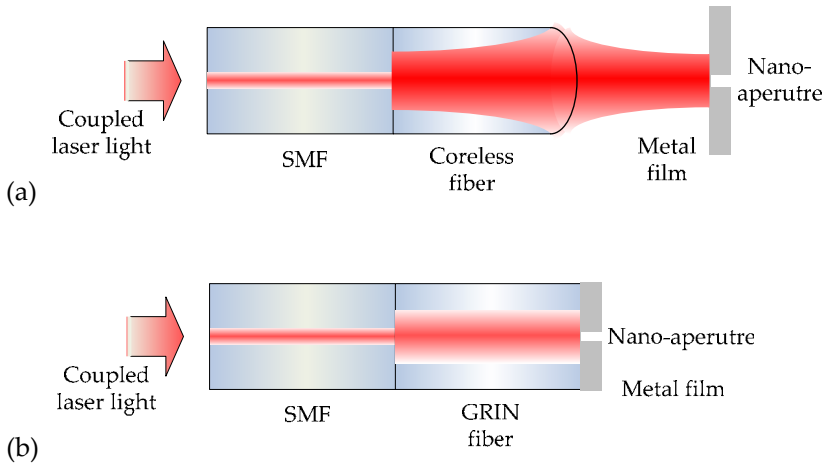

Fig. 3.1-1 The optical model of (a) freestanding case (b) integrated case

3.1.2 Parameters

The notations of the C-aperture dimensions are plotted in Fig. 3.1-2. Besides, a further parameter, named aspect ratio (AR), is defined as the ratio of the aperture width *b* to aperture length *a*.

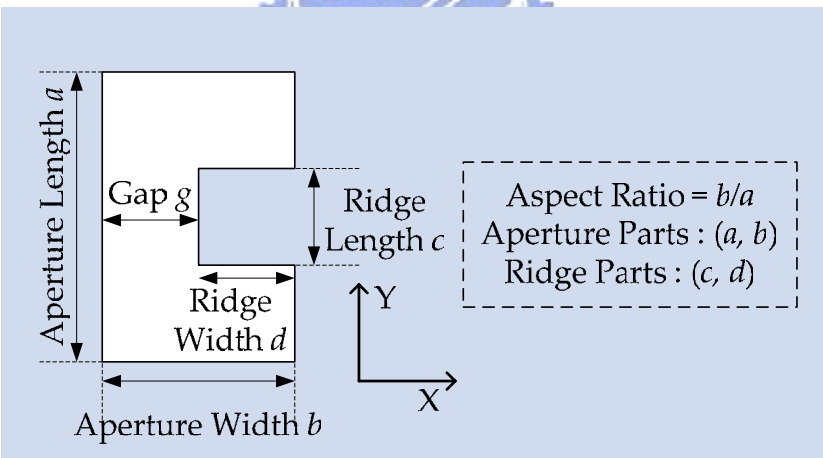

Fig. 3.1-2 Parameters of the C-aperture

3.1.3 Evaluation Factors

Power throughput (PT) is dimensionless and defined as the ratio of the total transmitted power to the product of incident power density and the aperture area.

$$PT=\frac{\text{Total transmitted power}}{\text{Incident power density}\times\text{Aperture area}}$$

Its physical meaning is to quantify the photon capturing ability of the aperture. PT less than unity indicates the photons even impinging on the aperture cannot tunnel through the aperture whereas excess over unity signifies those incident photons beyond the aperture area can still be captured, as schematically plotted in Fig. 3.1-3.

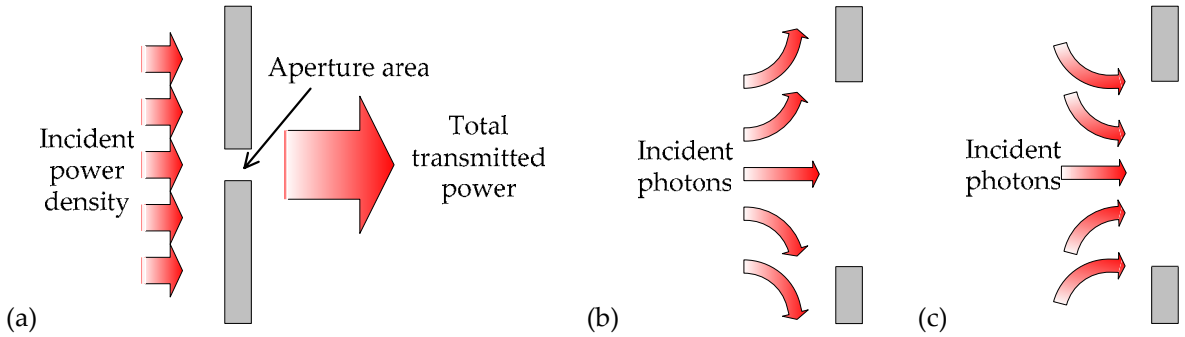

Fig. 3.1-3 Schemes of (a) power throughput, (b) photons incapable of tunneling and (c) photons captured by the aperture

Power throughput density (PTD), of which the unit is reciprocal of area, is defined as the ratio of power throughput to the spot size.

$$\text{PTD} = \frac{\text{Power throughput}}{\text{Spot size } S_x \times \text{ Spot size } S_y}$$

Spot size is the area that tunneled photons spread out and can be considered as the photon delivering ability of the aperture accordingly. From this perspective, PTD can be interpreted as

$$\text{PTD} = \frac{\text{Photon capturing ability}}{\text{Photon delivering ability}}$$

Therefore, PTD can evaluate the optical performance of an aperture thoroughly because it takes incidence and emission conditions into account concomitantly.

3.2 Results (1) – Freestanding Case

3.2.1 Square Aperture

In the beginning, a conventional square aperture was simulated in order to provide a reference to the improvement of the C-aperture. In this case, power throughput, as shown in Fig. 3.2-1, is increased quartically with the aperture size and the fitted polynomial reveals that Bethe's formula can only roughly estimate its tendency. The exact relation between the aperture size and the power throughput obviously requires much modification as a result of the dissimilarity between silver and a perfect conductor in visible light range.

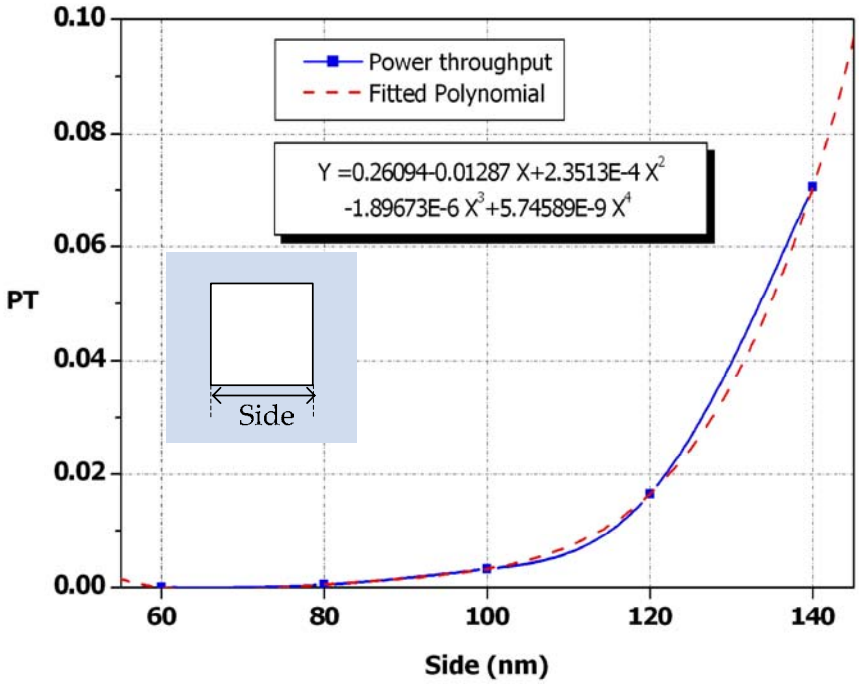

Fig. 3.2-1 Power throughput of various square apertures with the parameters shown in the inset

Due to the X-polarized incident light, the spot size is broadened in X-direction but oscillates only slightly in Y-direction, as listed in Table 3.2-1. The power throughput density, as plotted in Fig. 3.2-2, has resembling behaviors to the power throughput, indicating the spot size is approximately linearly proportional to the aperture size.

Table 3.2-1 Spot size of various square apertures

Side (nm*nm)	Spot Size (nm)	
	X	Y
60*60	147	111
80*80	164	108
100*100	185	125
120*120	222	138
140*140	231	133

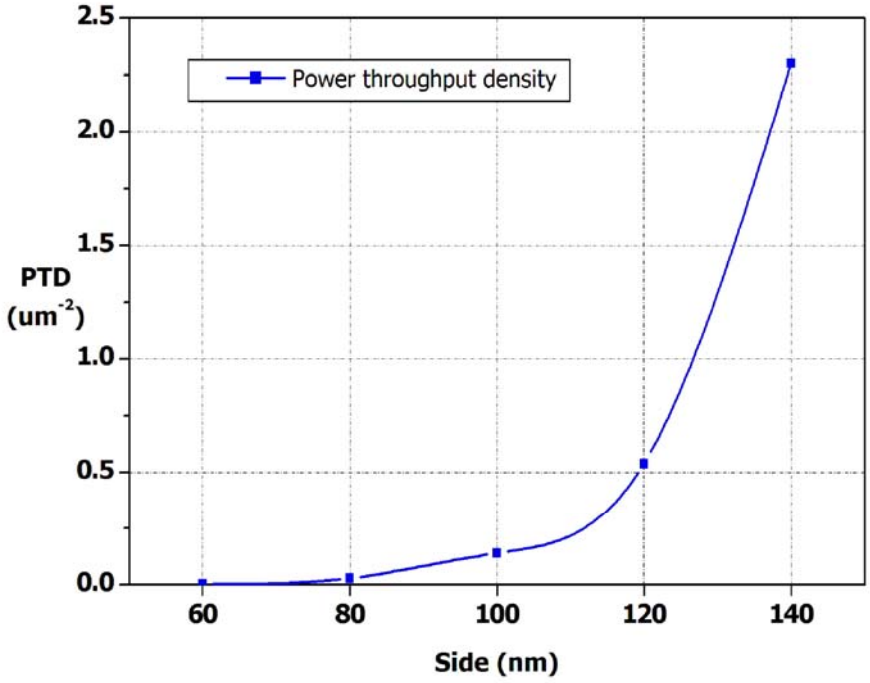

Fig. 3.2-2 Power throughput density of various square apertures

3.2.2 C-aperture with Fixed Aperture Parts

As the first step to optimize the C-shaped aperture, the aperture parts *a* and *b* were fixed as 210 nm and 84 nm; the ridge length *c* and gap *g* were variables. The power throughput as functions of *c* and *g*, as shown in Fig. 3.2-3, reveals that gap *g* is a critical parameter but ridge length *c* has an only minor impact owing to the similar tendency of these curves. Besides, the sharp decline with gap *g* smaller than 38 nm signifies the existence of a "cut-off gap" to be 38 nm, which is unchanged regardless of ridge length *c*.

As for the spot size, its variations in both X- and Y-directions are within 20 nm. In substance, the spot size is reduced with a narrower gap g but slightly oscillates with ridge length c, as listed in Table 3.2-2.

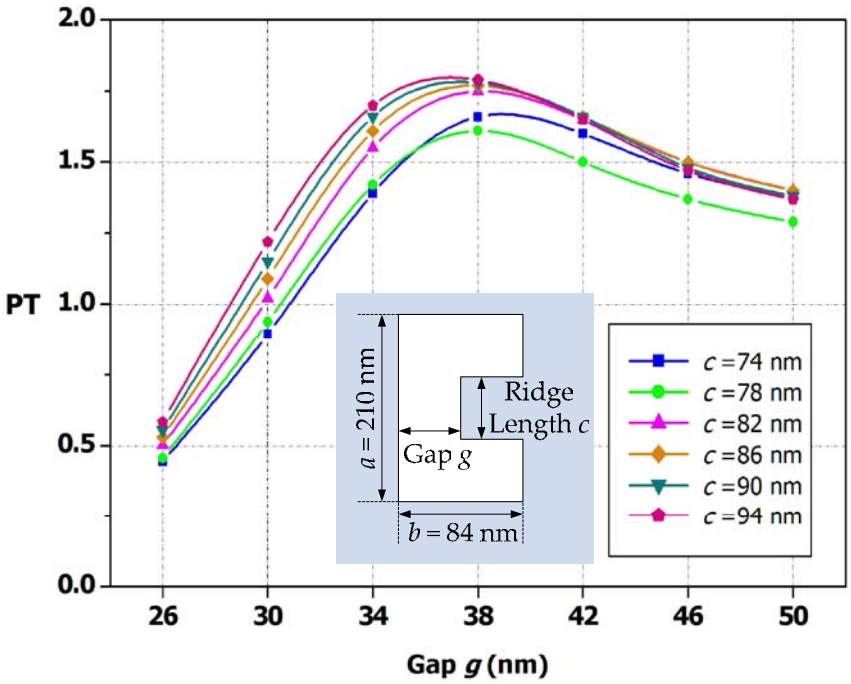

Fig. 3.2-3 Power throughput of the C-apertures with the parameters shown in the inset

Table 3.2-2 Spot size of the C-apertures in (a) X- and (b) Y-directions

(a)

Ridge width c (nm) \ Gap g (nm)	26	30	34	38	42	46	50
74	111.8	111.0	112.2	117.8	117.6	119.6	125.0
78	111.8	111.0	112.2	114.0	117.6	119.6	135.0
82	111.8	111.0	115.6	117.8	121.8	119.6	135.0
86	114.4	114.0	119.0	117.8	117.6	124.2	135.0
90	114.4	114.0	115.6	117.8	117.6	124.2	135.0
94	114.4	114.0	119.0	117.8	121.8	124.2	135.0

(b)

Ridge width c (nm) \ Gap g (nm)	26	30	34	38	42	46	50
74	129.2	129.2	129.2	136.0	136.0	136.0	136.0
78	132.0	132.0	132.0	132.0	132.0	132.0	132.0
82	134.4	134.4	134.4	134.4	140.8	140.8	140.8
86	136.4	136.4	136.4	136.4	136.4	142.6	142.6
90	132.0	132.0	144.0	144.0	144.0	144.0	144.0
94	139.2	139.2	139.2	139.2	139.2	139.2	145.0

The power throughput density, plotted in Fig. 3.2-4, has a similar behavior to the power throughput owing to the little variation in the spot size; consequently, the power throughput plays a more decisive role in this case.

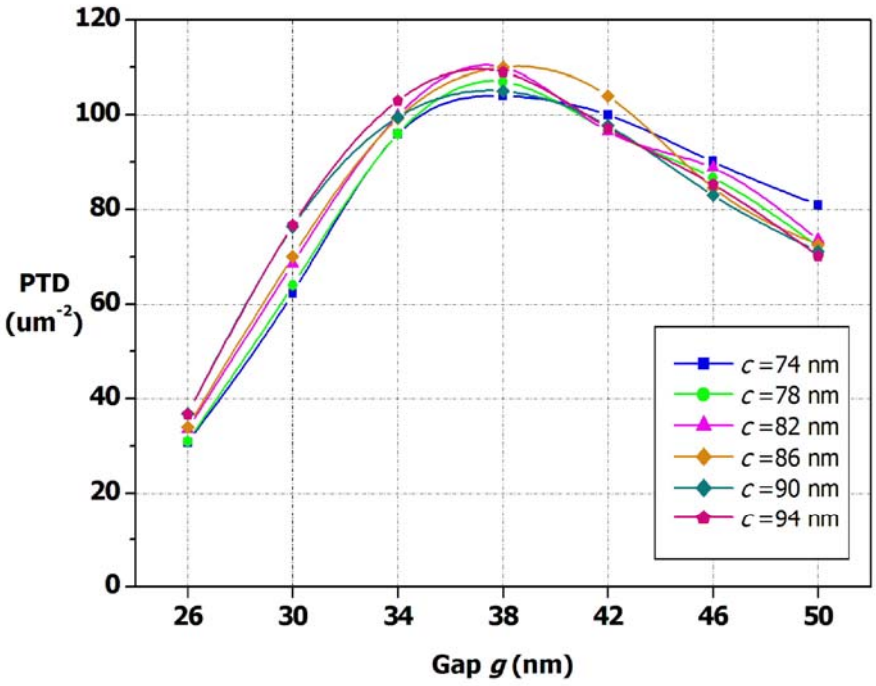

Fig. 3.2-4 Power throughput density of the C-apertures

3.2.3 C-aperture with Fixed Ridge Parts

Next, the variables were changed to aperture length *a* and aspect ratio AR; ridge parts *c* and *d* were kept 46 nm and 86 nm individually. Each curve of power throughput with different aperture length *a* reaches its maximum at aspect ratio of ~0.4, as shown in Fig. 3.2-5, implying aspect ratio is a crucial factor to transmission. This property rudimentarily characterizes a C-aperture as a single ridge waveguide.

Additionally, the more gradual undulation with larger aperture length *a* is attributable to the shrunk proportion that ridge parts occupy; as a result, the C-aperture appears as a rectangular aperture and the "cut-off" effect is suppressed accordingly.

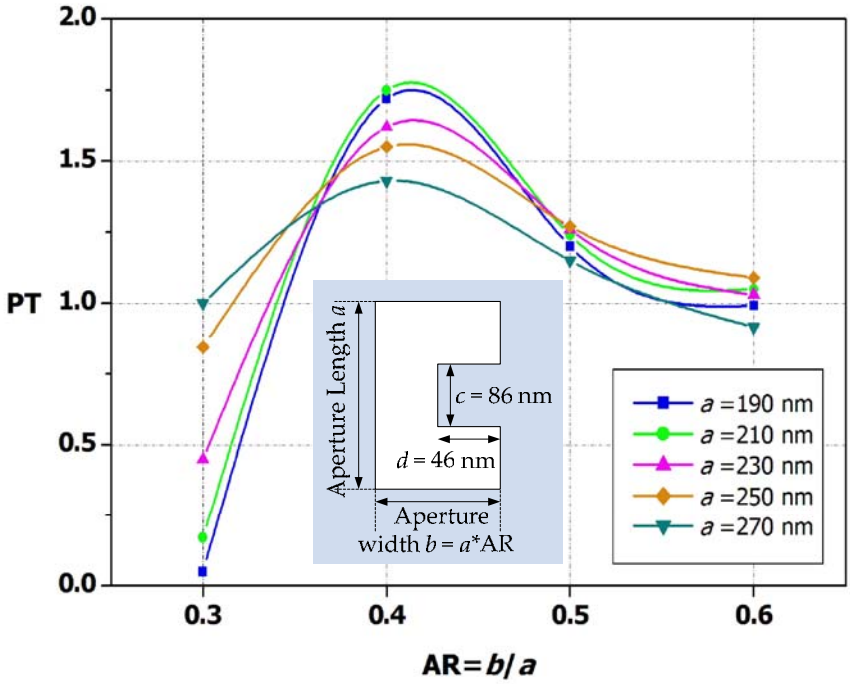

Fig. 3.2-5 Power throughput of the C-apertures with the parameters shown in the inset

Since gap g can be expressed as

$$g = a \times \mathrm{AR} - 46 ,$$

the smaller aperture length a and aspect ratio AR will result in narrower gap g. Therefore, referring to Table 3.2-3, the spot size is reduced with smaller gap g in X-direction and alters to a small extent in Y-direction. This phenomenon is parallel to section 3.2.2.

Compared to the power throughput, those peaks of the power throughput density at aspect ratio of 0.4 become more discernible, as shown in Fig. 3.2-6, which is in virtue of that spot size reduction is more apparent than power throughput enhancement.

Table 3.2-3 Spot size in (a) X- and (b) Y-directions of C-apertures

(a)

Aperture length *a* (nm) \ Aspect Ratio AR	0.3	0.4	0.5	0.6
190	108.9	111.0	122.5	122.4
210	107.1	117.8	123.9	136.0
230	115.0	128.8	131.1	128.8
250	116.0	129.6	150.1	145.6
270	119.0	130.2	142.4	139.2

(b)

Aperture length *a* (nm) \ Aspect Ratio AR	0.3	0.4	0.5	0.6
190	130.0	130.0	135.2	135.2
210	130.2	136.4	142.6	142.6
230	136.8	144.0	144.0	144.0
250	147.6	147.6	155.8	147.6
270	147.2	147.2	147.2	147.2

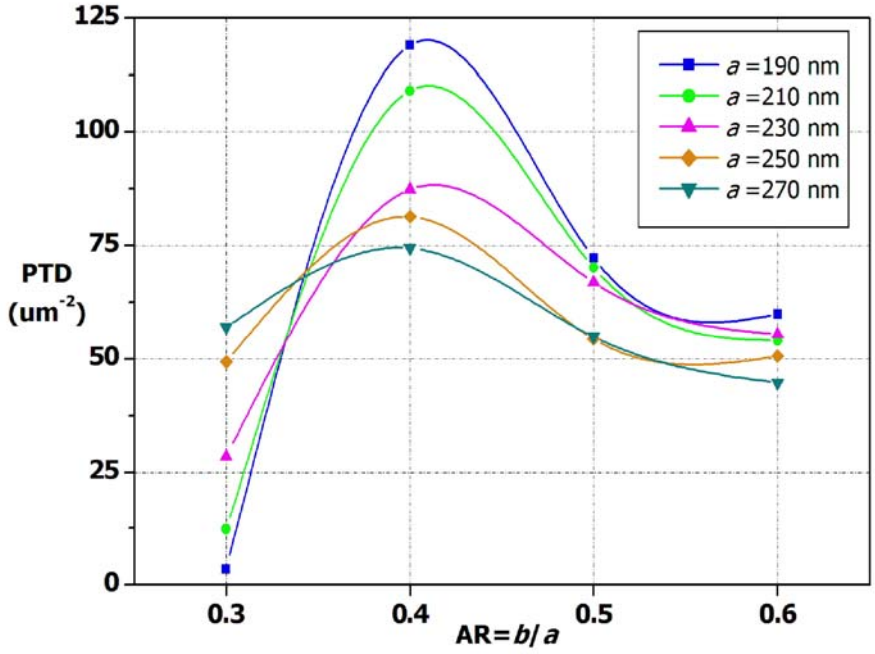

Fig. 3.2-6 Power throughput density of C-apertures

3.2.4 Correspondence Relation

The analogy between a C-aperture and a single ridge waveguide is an impetus to explore a more fundamental relationship between maximum transmission and the C-aperture dimensions. According to the aforementioned simulation results, it

cannot refrain from conjecturing that whether a fixed ridge width *d* corresponds to a specific aspect ratio AR where the maximum power throughput takes place.

Because ridge length *c* has a minor effect on the power throughput (please refers to section 3.2.2), here *c* was kept 86 nm. With different ridge width *d*, the identical procedures to those in section 3.2.3 were repeated, and the C-aperture dimensions and simulation results are juxtaposed in Fig. 3.2-7.

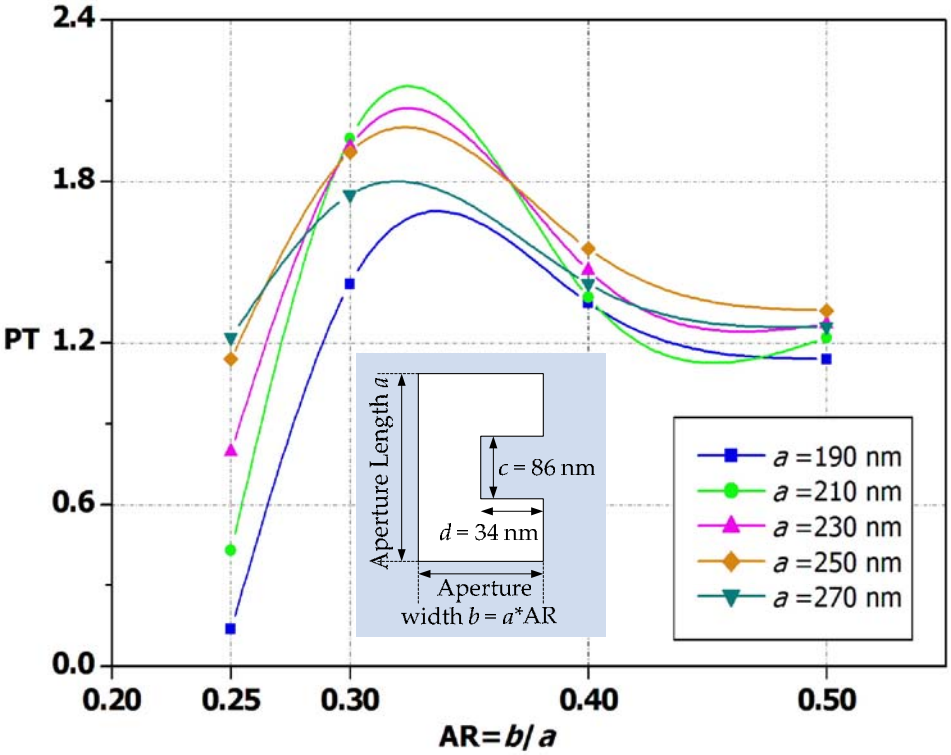

(a)

Fig. 3.2-7 Power throughput of the C-apertures with (a) *d*=34 nm

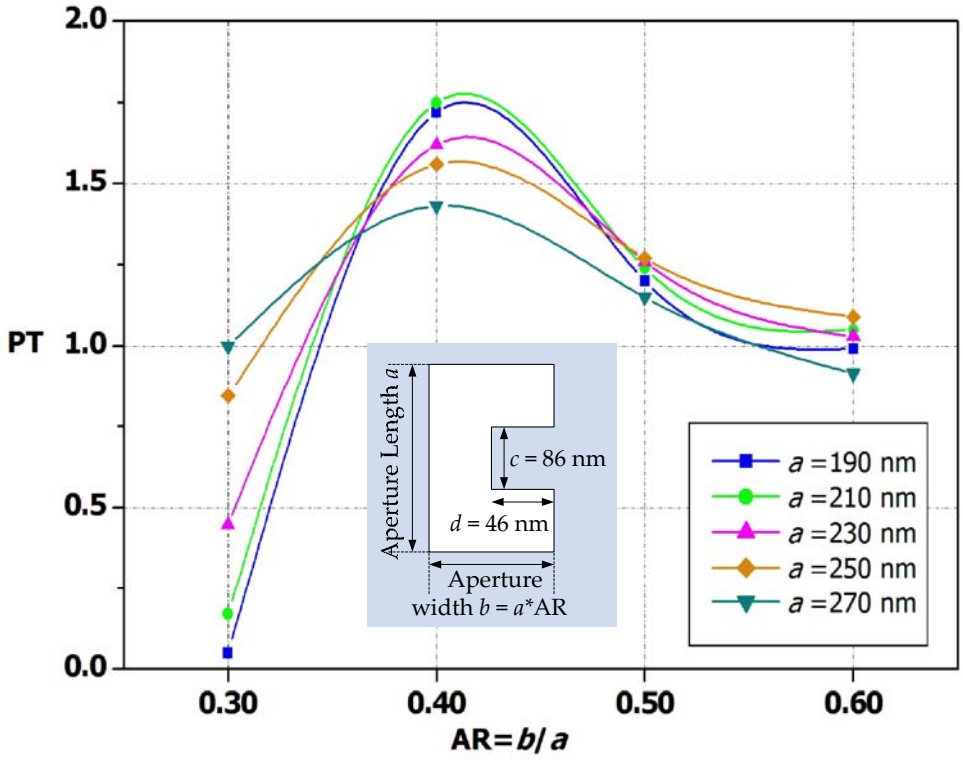

(b)

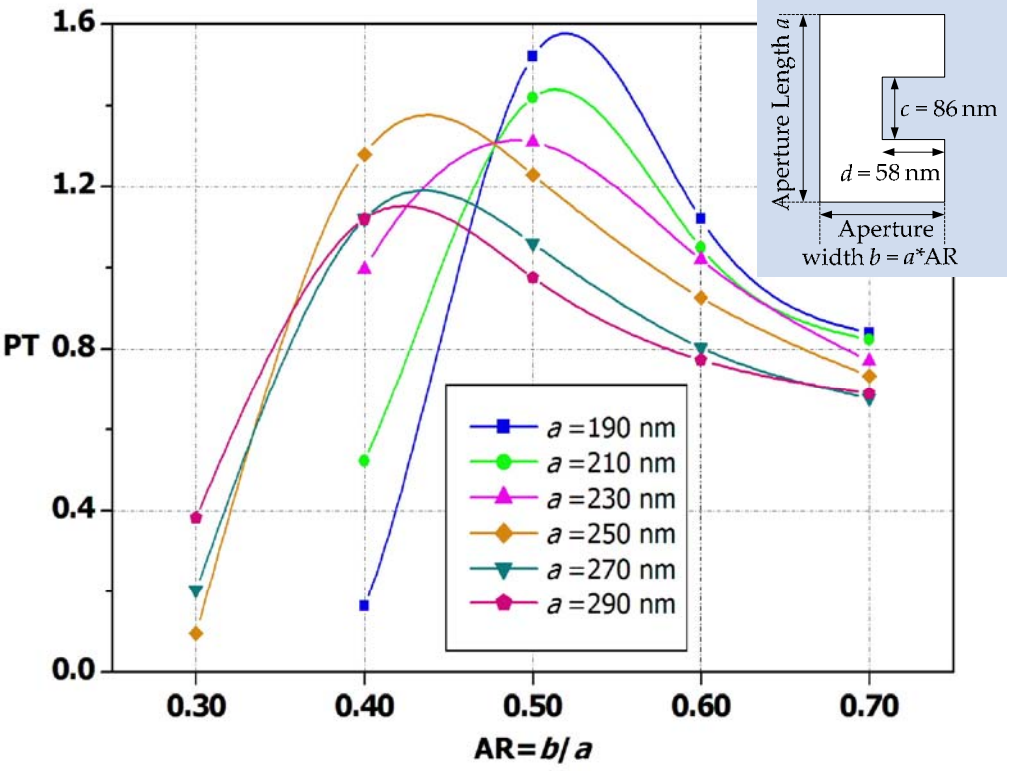

(c)

Fig. 3.4-7 Power throughput of the C-apertures with (b) *d*=46 nm and (d) *d*=58 nm

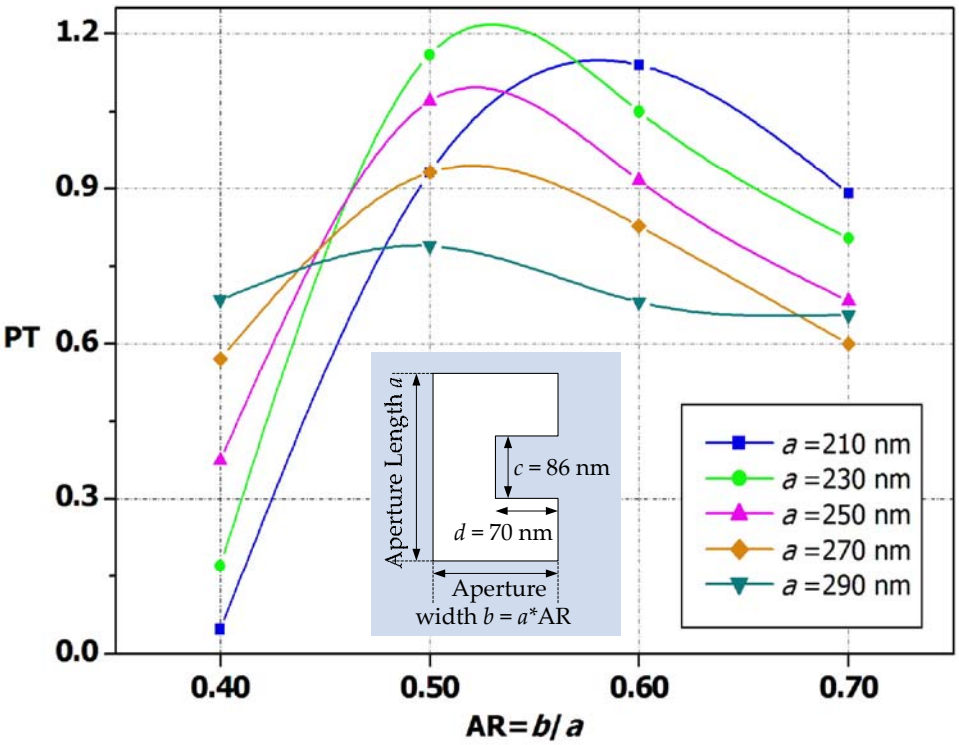

(d)

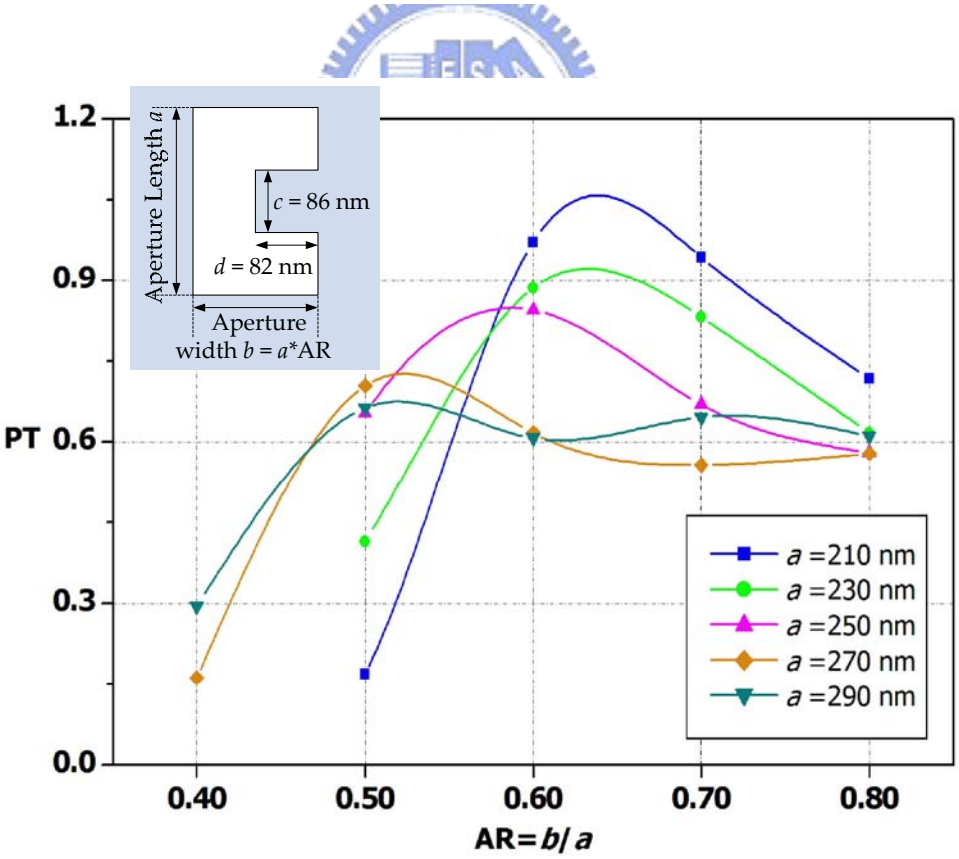

(e)

Fig. 3.2-7 Power throughput of C-apertures with (d) *d*=70 nm and (e) *d*=82 nm

In the following statements, the aspect ratio AR that the peak corresponds to is denoted by AR_{peak} for convenience. The AR_{peak} of each curve are selected narrowly and summed up in Table 3.2-4. It can be found that the AR_{peak} grows larger with wider ridge width d in general; however, observing each diagram in Fig. 3.2-7 carefully, the peaks shift towards to larger AR_{peak} in sort of the magnitude of aperture length a.

Table 3.2-4 AR_{peak} of each curve in Fig. 3.2-7

Aperture length a (nm) \ Ridge width d (nm)	34	46	58	70	82
190	0.330	0.415	0.515		
210	0.310	0.415	0.510	0.590	0.630
230	0.310	0.415	0.500	0.520	0.625
250	0.310	0.410	0.425	0.520	0.600
270	0.300	0.405	0.425	0.515	0.520
290			0.420	0.500	0.520

Since gap g is a critical factor to transmission through the C-aperture, it is reasoned that the gap may plays an important role in the relation between maximum power throughput and C-aperture dimensions; hence, the gap corresponding to each AR_{peak} are calculated and listed in Table 3.2-5 as well.

Table 3.2-5 The gap corresponding to each AR_{peak} in Table 3.2-4

Aperture length a (nm) \ Ridge width d (nm)	34	46	58	70	82
190	28.70	32.85	39.85		
210	31.10	41.15	49.10	53.90	50.30
230	37.30	49.45	57.00	49.60	61.75
250	43.50	56.50	48.25	60.00	68.00
270	47.00	63.35	56.75	69.05	58.40
290			63.80	75.00	68.80

After painstaking calculation, a quantity computed by a simple formula:

$$\frac{(\text{Gap } g)\times\ (\text{Ridge width } d)}{(\text{Aperture width } b)^2} \quad \text{----(1)}$$

shows amazingly great consistency as recited in Table 3.2-5. Their average value is 0.247 and the standard deviation is only $3.51*10^{-3}$.

Table 3.2-6 The quantity of each peak computed by equation (1)

Aperture length a (nm) \ Ridge width d (nm)	34	46	58	70	82
190	0.248	0.243	0.241		
210	0.250	0.249	0.248	0.246	0.236
230	0.249	0.250	0.250	0.243	0.245
250	0.246	0.247	0.248	0.249	0.248
270	0.244	0.244	0.250	0.250	0.243
290			0.249	0.250	0.248
Average	***0.247***				
Standard Deviation	***3.51E-03***				

Therefore, it is inferred that the C-aperture dimensions should meet a "correspondence relation" as:

$$\frac{(\text{Gap } g)\times(\text{Ridge width } d)}{(\text{Aperture width } b)^2}\cong 0.247$$

in order to reach the local maximum power throughput. The contribution of this correspondence relation is to render a feasible foundation for a C-aperture design to achieve local maximal power throughput.

3.2.5 Comparison (1) – Normal Incidence

Here a $60*60$ nm^2 square aperture is taken as the reference because its spot size is in a similar scale to the C-aperture. From Table 3.2-7, the C-aperture with dimensions (a, b, c, g) of (210, 84, 86, 46) nm affords power throughput enhanced by a factor of $2.78*10^4$, leading to its power throughput density is $2.80*10^4$ times greater than the square aperture. Examining the electric field energy distributions can explicitly manifest the improvement of the C-aperture, as shown in Fig. 3.2-8, where the amplitudes of the electric field energy density are vastly different.

Furthermore, inspecting the field distribution of the C-aperture in Fig. 3.2-8(b) will found that most of the transmitted energy is confined in the area formed by the ridge length *c* and gap *g*. This suggests that the gap critically determines the power throughput and defines the spot size of the C-aperture, which is another characteristic of a single ridge waveguide.

Table 3.2-7 Comparison of a 60*60 nm² square aperture and the optimum C-shaped aperture

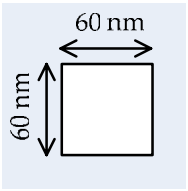

Square	Aperture type	C-shaped
6.42E-05	**Power throughput**	1.77E+00
147*111	**Spot size (nm*nm)**	117.8*136.4
3.93E-03	**Power throughput density**	1.10E+02

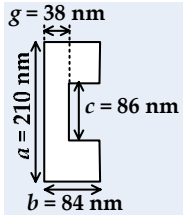

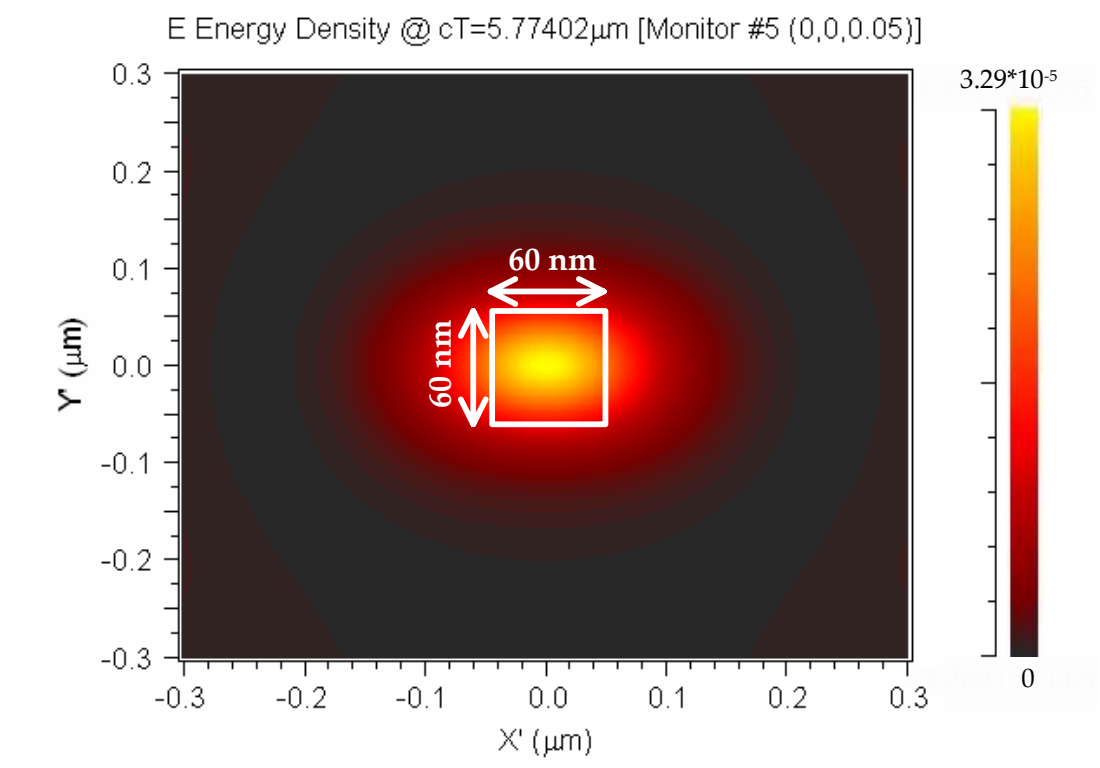

(a)

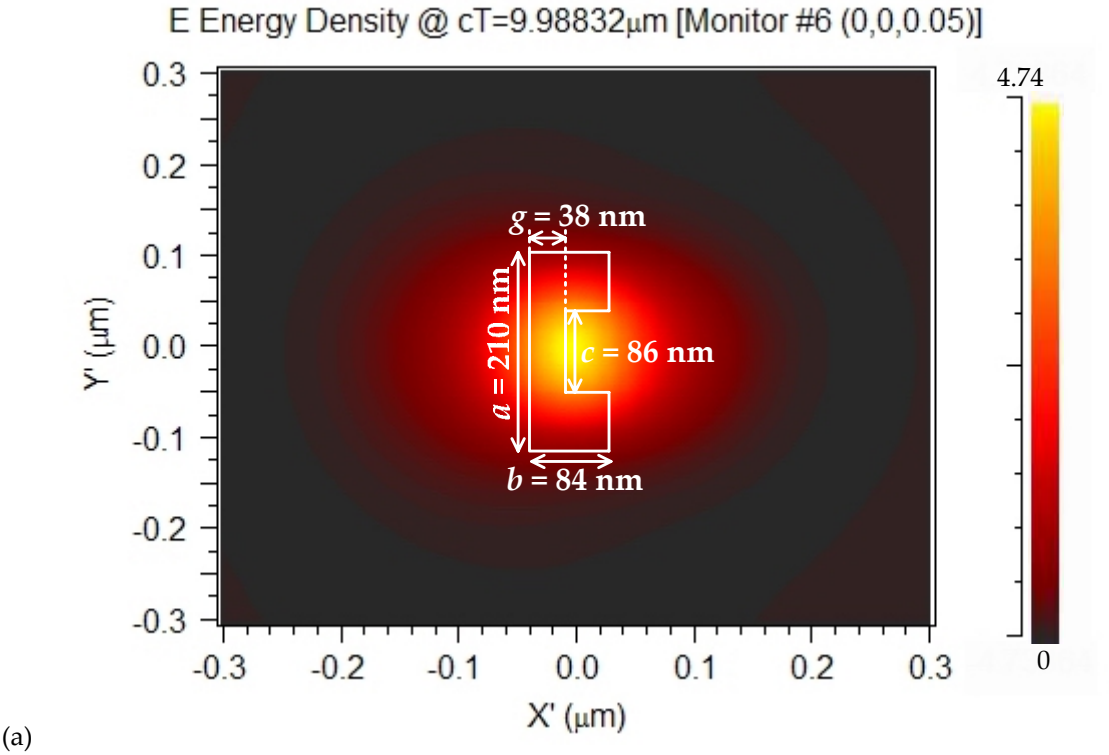

(b)

Fig. 3.2-8 Electric field energy density of (a) a 60*60 nm² square aperture and (b) the optimum C-aperture, the shape and dimensions of the apertures are outlined and labeled. Note different color scale in each diagram.

This unusual high power throughput of the C-aperture involves two physical meanings. On the one hand, PT over unity stands for that the incident photons not impinging on the aperture are also captured, accompanying a "funnel" effect to take place in front of the aperture. On the other hand, high power throughput is attributable to the existence of the propagation mode which the square aperture lacks. This is analogous to a single ridge waveguide that can allow of propagation modes, which may be forbidden in a conventional rectangular waveguide. Therefore, the energy can be propagated after tunneling through the C-aperture, whereas that carried by an evanescent wave attenuates exponentially and the energy is confined within only several nanometers from the aperture accordingly.

3.2.6 Oblique Incidence

The C-aperture in freestanding film can be combined with a solid immersion lens; thus, the optical performance under oblique incidence is taken into accounts. The oblique incident angle in XZ plane and YZ plane with respect to positive Z axis are defined as phi (Φ) and theta (θ) respectively; further, the definition of positive and negative angle is schematically sketched in Fig. 3.2-9(a). In this case, the C-aperture dimension is the optimum one mentioned in section 3.2.5, as plotted in 3.2-9(b).

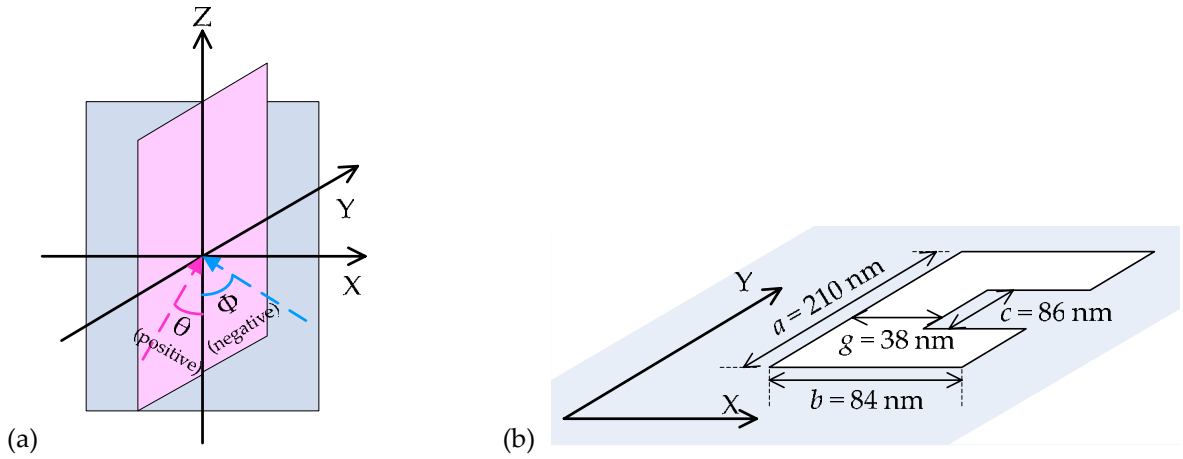

Fig. 3.2-9 (a) Definition of incident angle phi (Φ) and theta (θ) and (b) the C-aperture dimensions

The power throughput as a function of Φ can be fitted by a Gaussian function almost perfectly as shown in Fig. 3.2-10. With negative Φ, power throughput is further increased and can reach up to 2.58 at -27°, which is a factor of 1.5 of that at normal incidence; however, the spot size is nearly unaffected by oblique incidence, as listed in Table 3.2-8. Thereby, one can expect that the power throughput density is also improved to an identical extent as the power throughput.

Table 3.2-8 Spot size at different incident angle Φ

Φ	Spot size (nm)	
	X	Y
-45	117.8	142.6
-42	117.8	136.4
-39	117.8	136.4
-36	117.8	136.4
-33	117.8	136.4
-30	117.8	136.4
-27	117.8	136.4
-24	121.6	142.6
-21	121.6	142.6
-18	121.6	142.6
-15	121.6	142.6
-12	121.6	142.6
-9	121.6	142.6
-6	117.8	136.4
-3	117.8	136.4
0	117.8	136.4
3	117.8	136.4
6	117.8	142.6
9	121.6	142.6
12	117.8	136.4
15	117.8	136.4

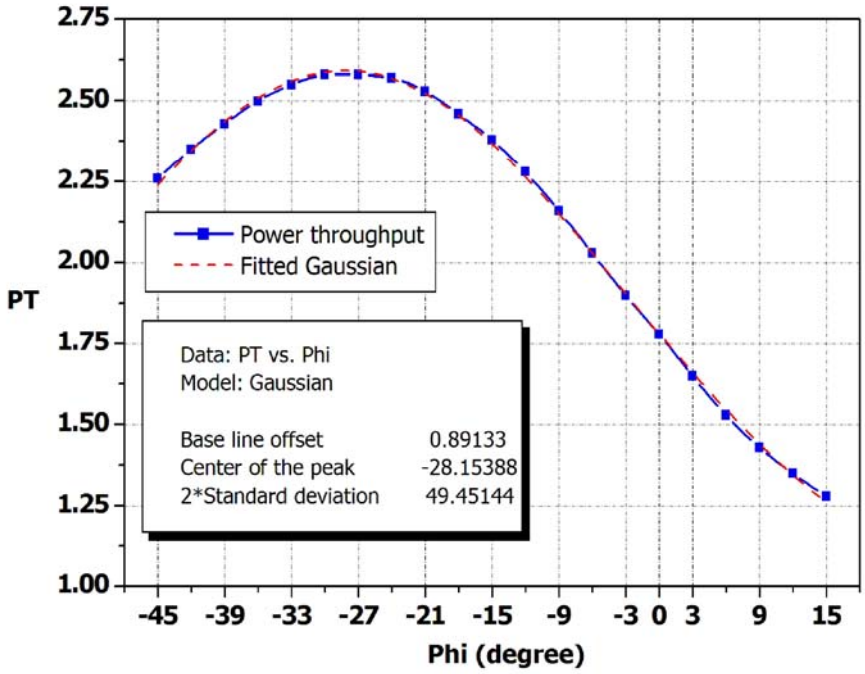

Fig. 3.2-10 Power throughput as a function of incident angle Φ

On the other hand, the dependence of power throughput on θ, as displayed in Fig. 3.2-11, is also agreed with a Gaussian function. The power throughput is only slightly affected by the alternation of θ, and its peak at 0° is reasonable due to the symmetry of the C-aperture along Y direction. Besides, this oblique incident angle does not work upon the spot size at all as recited in Table 3.2-9.

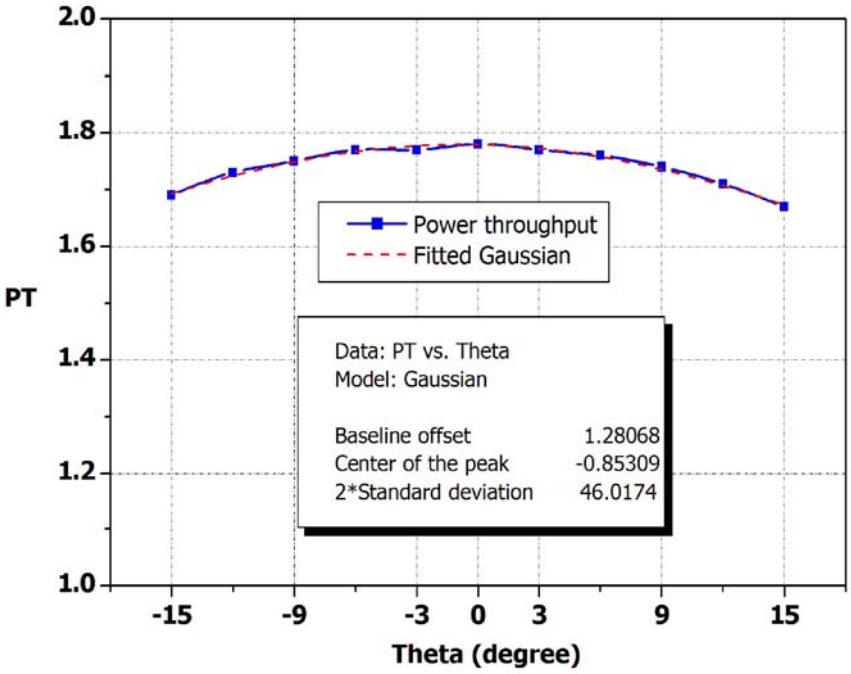

Fig. 3.2-11 Power throughput as a function of incident angle θ

Table 3.2-9 Spot size at different incident angle θ

θ	Spot size (nm)	
	X	Y
-15	117.8	136.4
-12	117.8	136.4
-9	117.8	136.4
-6	117.8	136.4
-3	117.8	136.4
0	117.8	136.4
3	117.8	136.4
6	117.8	136.4
9	117.8	136.4
12	117.8	136.4
15	117.8	136.4

3.2.6 Comparison (2) – Oblique Incidence

According to the above-mentioned simulation results, power throughput and optical performance can be further improved with oblique incident angle (Φ, θ) of (-27°, 0°). Under such incident condition and compared to a 60*60 nm^2 square aperture, the C-aperture possesses a factor of 4.02*10^4 and 4.10*10^4 in power throughput and power throughput density respectively, as listed in Table 3.2-7.

Table 3.2-10 Comparison of a 60*60 nm^2 square aperture and the optimum C-aperture under incident angle (Φ, θ) of (-27°, 0)

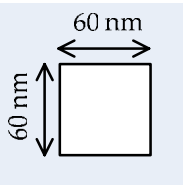

Square	Aperture type	C-shaped
6.42E-05	**Power throughput**	2.58E+00
147*111	**Spot size (nm*nm)**	117.8*136.4
3.93E-03	**Power throughput density**	1.61E+02

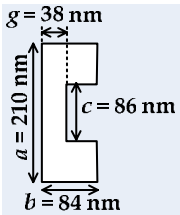

3.3 Results (2) – Integrated Case

3.3.1 Square Aperture

Now, transfer the attention to the other model – the integrated case. The square aperture on the fiber tip is also simulated first to be the reference.

Power throughput, spot size and power throughput density are shown in Fig. 3.3-1, Table 3.3-1 and Fig. 3.3-2 respectively. Generally speaking, the optical behaviors resemble greatly to that in the freestanding case (please refer to section 3.2.1); the slight difference is caused by the reduced incident wavelength of ~430 nm owing to the mean refractive index of the GRIN fiber of ~1.475.

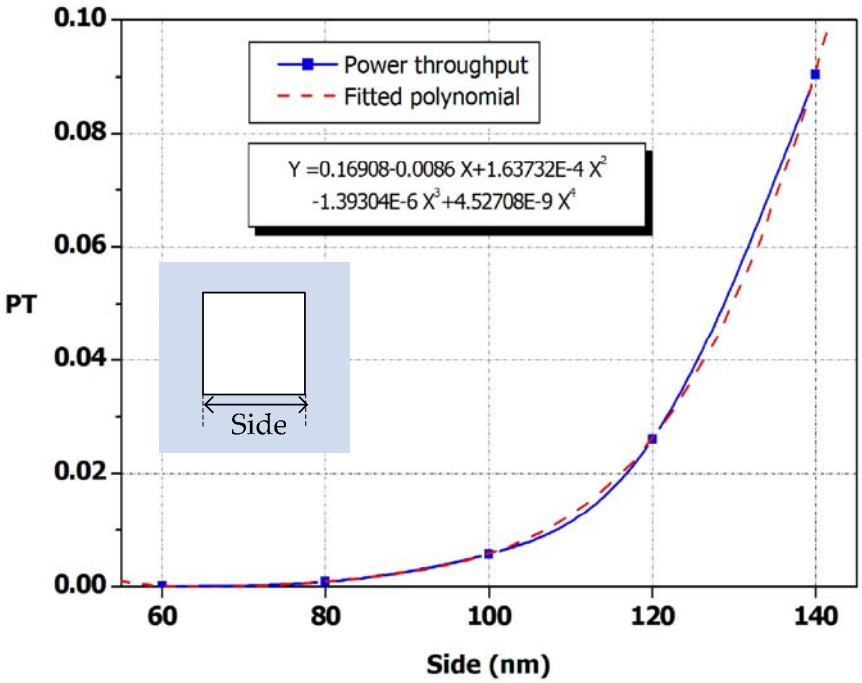

Fig. 3.3-1 Power throughput of various square apertures

Table 3.3-1 Spot size of various square apertures

Side (nm*nm)	Spot Size (nm)	
	X	Y
60*60	147	105
80*80	164	108
100*100	185	125
120*120	210	126
140*140	252	147

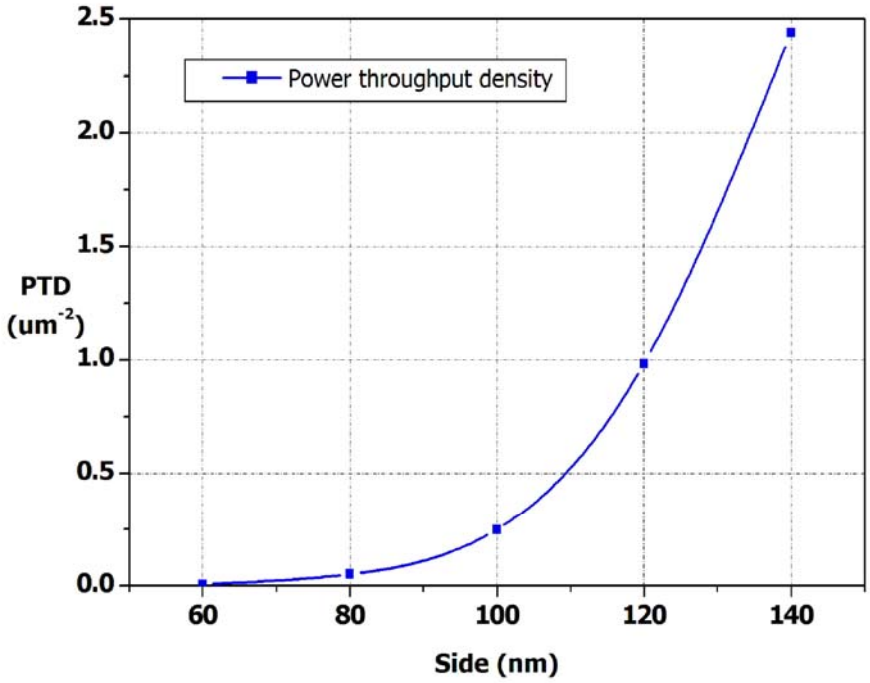

Fig. 3.3-2 Power throughput density of various square apertures

3.3.2 Index Matching

Due to the reduced wavelength, the C-aperture dimensions should be adjusted. For an ordinary single ridge waveguide, it is more meaningful to express its dimensions normalized to wavelength than the absolute values. The aforementioned analyses suggest some analogies between a single ridge waveguide and a C-aperture; moreover, the incident frequency remains constant so that the optical property of the metal is unchanged. Therefore, an inspiration – downsizing the optimum C-aperture design of the freestanding case in section 3.2 – was stimulated, as schematically illustrated in Fig. 3.3-3.

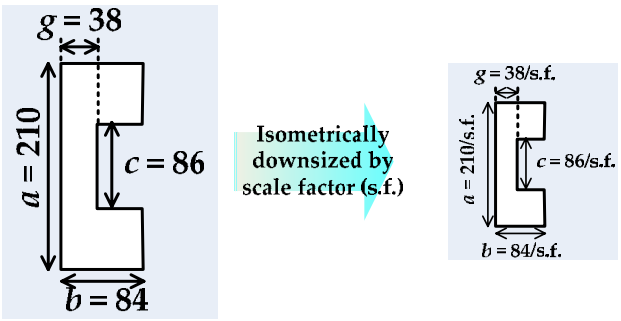

Fig. 3.3-3 Diagrams of isometric downsizing, all dimensions are in units of nm

In order to demonstrate this concept, the first step was to isometrically downsize the optimum C-aperture in the freestanding case by a varied scale factor ranging from 1.1 to 1.475 (1.475 is the mean refractive index of GRIN fiber). The solid line in Fig. 3.3-4 reveals the power throughput is not as good as that in the freestanding case until the scale factor is approximated to 1.475. Therefore, the next step was to explore the power throughput of a downsized C-aperture with the scale factor equal to the refractive index of its substrate (index matching). As the dash line in Fig. 3.3-4 shows, index matching can provide satisfactory power throughput that exceeds over unity as the freestanding case. Consequently, to isometrically downsize the C-aperture by a scale factor of 1.475 provides a good starting point for the following simulation.

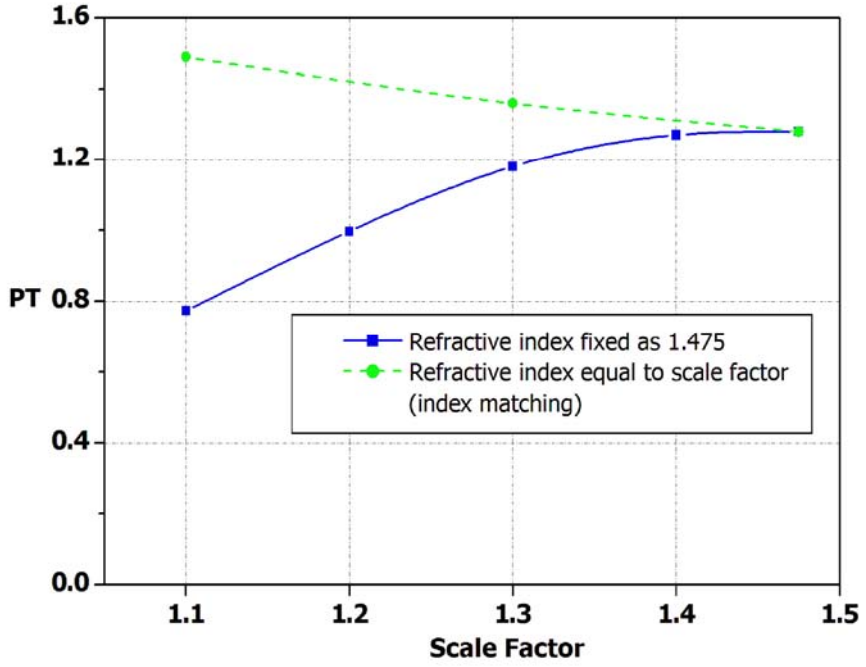

Fig. 3.3-4 Power throughput as a function of scale factor and different refractive index

3.3.3 C-aperture with Fixed Aperture Parts

The parameters of the C-aperture in this section are depicted in Fig. 3.3-5, where the aperture parts *a* and *b* were fixed while the gap *g* and ridge length *c* were varied.

Based on the index matching, gap g and ridge length c in this section comes from dividing those parameters in Fig. 3.2-3 by 1.475, as shown in Fig. 3.3-5.

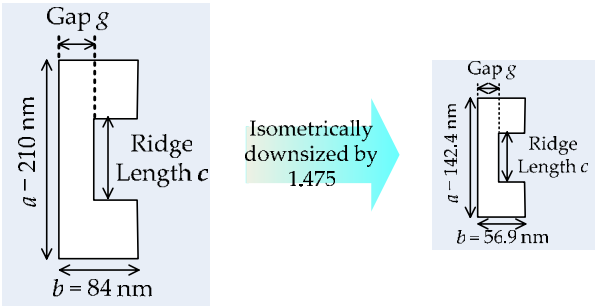

Fig. 3.3-5 Parameters of downsized C-aperture with varied ridge parts

In this case, "linear downsizing" effect emerges from the power throughput as shown in Fig. 3.3-6. Referring to the freestanding case (Fig. 3.2-3), it is easily observed that not only the tendency follows the same trend but the cut-off gap is linearly downsized to be 25.8 nm as well.

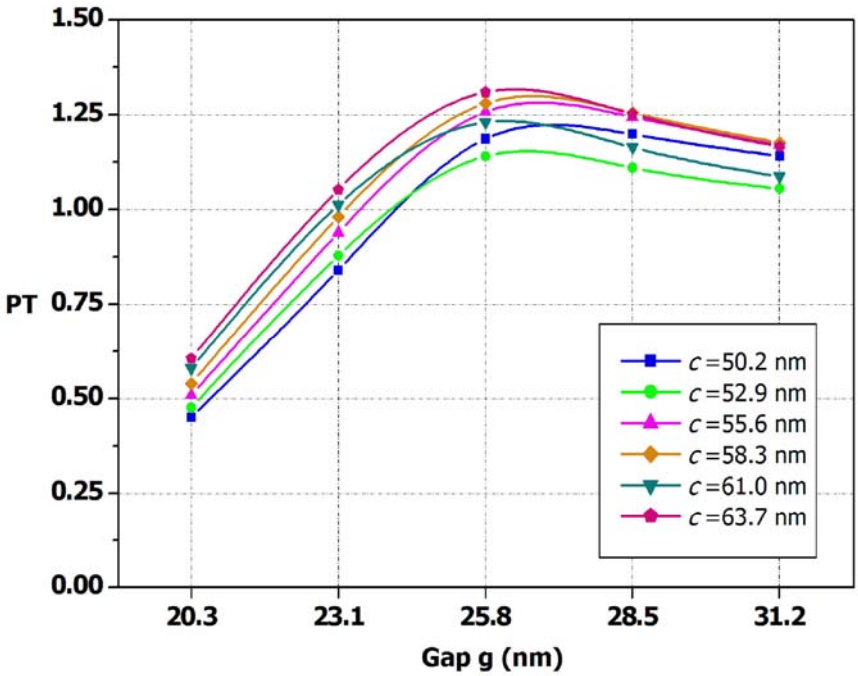

Fig. 3.3-6 Power throughput of the C-aperture with parameters as Fig. 3.3-5, ridge length c is chosen by downsizing those values in section 3.2-2 by 1.475

Compared to the freestanding case (Table 3.2-2), the C-aperture on fiber tip can provide a more reduced spot size with the diminution in X and Y direction of 10 nm and 30 nm respectively, as listed in Table 3.3-2. Finally, the calculated power throughput density is displayed in Fig. 3.3-7, of which the resemblance to the freestanding case (Fig. 3.2-4) is just anticipated.

Table 3.3-2 Spot size of the C-apertures on the fiber tip in (a) X and (b) Y directions

(a)

Ridge width *c* (nm) \ Gap *g* (nm)	**20.3**	**23.1**	**25.8**	**28.5**	**31.2**
50.2	101.7	106.0	103.1	102.5	112.3
52.9	101.7	99.1	103.1	105.4	112.3
55.6	101.7	103.7	103.1	111.1	112.3
58.3	101.7	103.7	108.2	111.1	112.3
61.0	103.7	99.1	108.2	108.2	112.3
63.7	101.7	106.0	105.6	108.2	112.3

(b)

Ridge width *c* (nm) \ Gap *g* (nm)	**20.3**	**23.1**	**25.8**	**28.5**	**31.2**
50.2	101.4	106.0	106.0	106.0	110.6
52.9	102.9	98.4	107.4	107.4	107.4
55.6	104.1	104.1	108.5	112.8	112.8
58.3	105.1	105.1	109.3	113.5	113.5
61.0	105.8	105.8	109.8	109.8	109.8
63.7	106.2	110.1	110.1	110.1	110.1

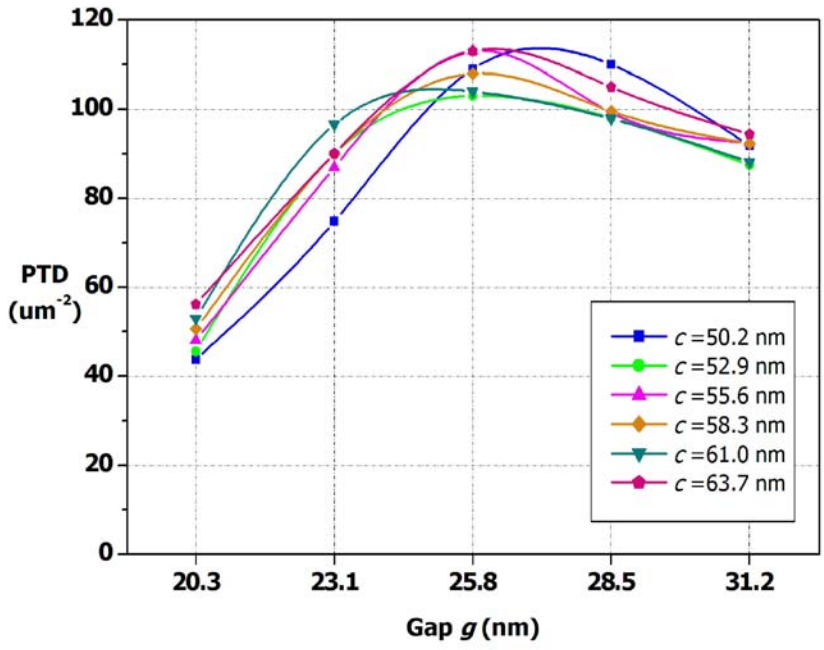

Fig. 3.3-7 Power throughput density of the C-apertures; the ridge length *c* is obtained by downsizing those values in section 3.2.2 by 1.475

3.3.4 C-aperture with Fixed Ridge Parts

Following the precedent, the parameters here is obtained by downsizing those in section 3.2.3 by 1.475, as shown in Fig. 3.3-8.

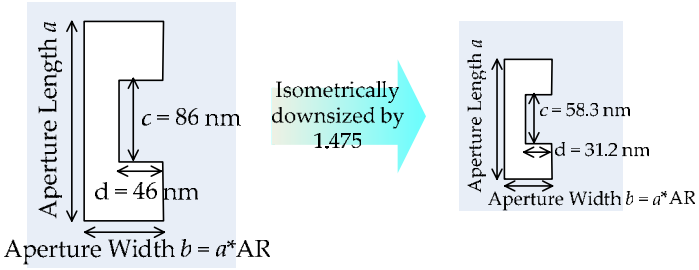

Fig. 3.3-8 Parameters of downsized C-aperture with varied aperture parts

In this case, the peaks of power throughput also occur at aspect ratio of 0.4 as shown in Fig. 3.3-9, signifying that the propagation condition can be reproduced while the C-aperture dimensions are normalized to the incident wavelength. This conspicuous feature assists the statement that a C-aperture can be treated as a single ridge waveguide.

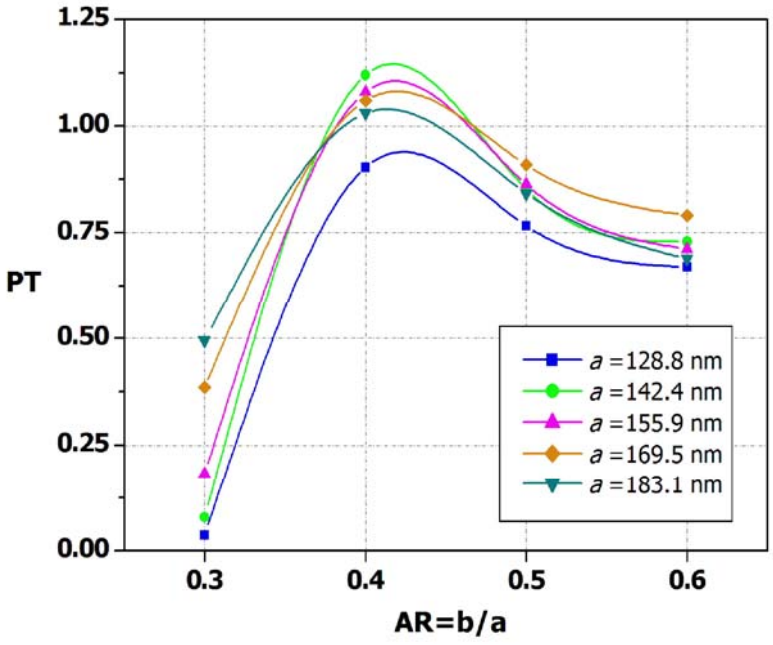

Fig. 3.3-9 Power throughput of the C-apertures with parameters as Fig. 3.3-8, the aperture length *a* is obtained by downsizing those values in section 3.2.3 by 1.475

The spot size listed in Table 3.3-3 is also much reduced in comparison with that of the freestanding case (Table 3.2-3); the power throughput density is calculated and displayed in Fig. 3.3-10.

Table 3.3-3 Spot size of the C-aperture on fiber tip in (a) X and (b) Y directions

(a)

Aperture length *a* (nm) \ Aspect Ratio AR	**0.3**	**0.4**	**0.5**	**0.6**
128.8	93.2	99.7	106.3	115.3
142.4	98.0	105.6	112.0	119.3
155.9	99.8	112.3	116.9	124.7
169.5	108.1	113.5	117.8	134.0
183.1	106.8	117.7	126.7	133.7

(b)

Aperture length *a* (nm) \ Aspect Ratio AR	**0.3**	**0.4**	**0.5**	**0.6**
128.8	95.2	102.5	102.5	102.5
142.4	104.1	108.5	108.5	112.8
155.9	110.4	110.4	110.4	110.4
169.5	119.6	113.9	119.6	119.6
183.1	114.7	121.1	121.1	121.1

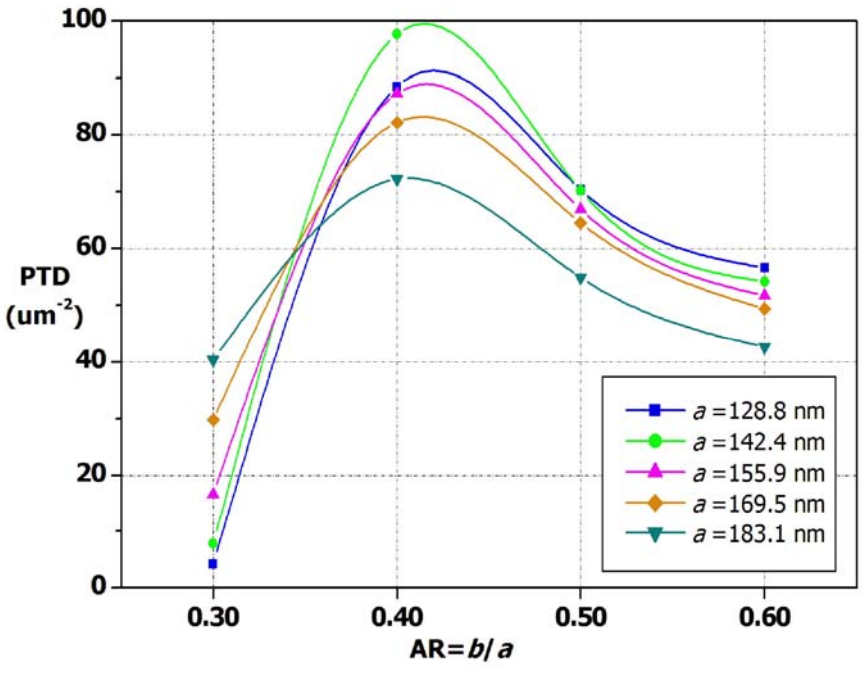

Fig. 3.3-10 Power throughput density of the C-apertures on fiber tip; the aperture length *a* is obtained by downsizing those values in section 3.2.3 by 1.475

In summary, for the freestanding case, the disparity of the spot size in X and Y direction is around 20 nm (Table 3.2-2 and 3.2-3), resulting in an inappropriate elliptical optical spot; however, the C-aperture integrated on the fiber tip can surmount this drawback. As indicated in Tables 3.3-2 and 3.3-3, the spot size in X and Y direction is closer to each other, where the difference can be controlled within 10 nm; therefore, a more circle-like tiny spot can be obtained in this model.

3.3.5 Correspondence Relation

In order to confirm the correspondence relation, the procedures identical to that in section 3.2.4 were adopted with downsizing those parameters in section 3.2.4 by 1.475. The C-aperture dimensions and simulation results are juxtaposed in Fig. 3.3-11.

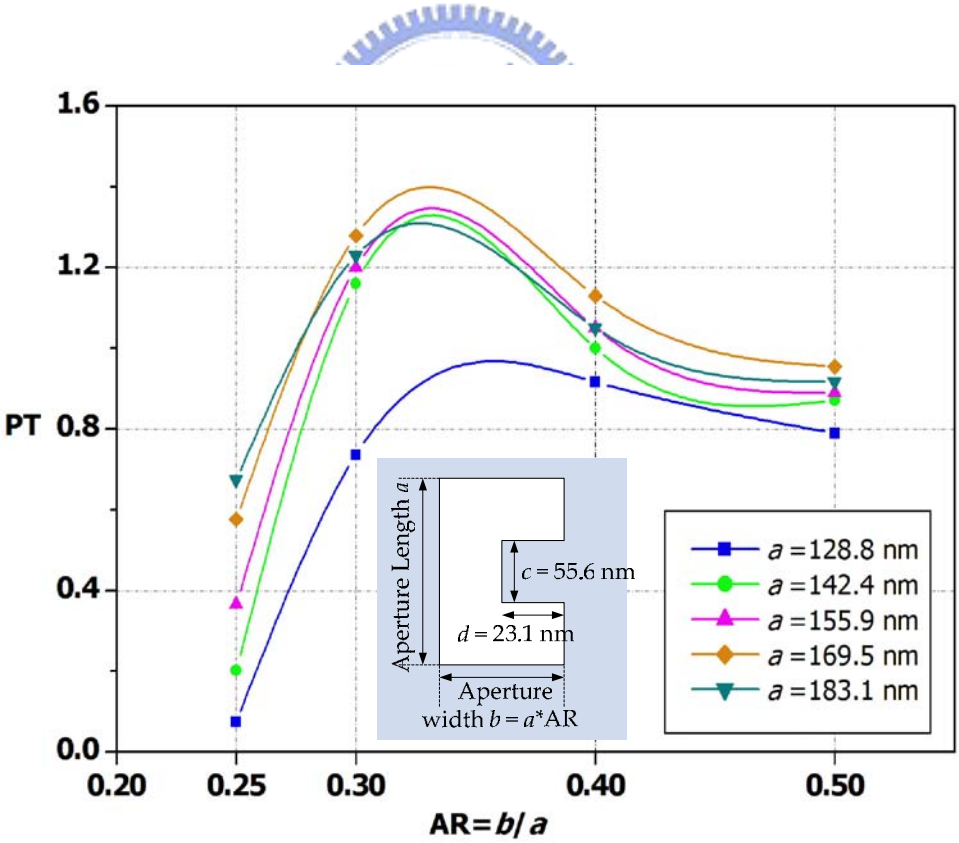

(a)

Fig. 3.3-11 Power throughput of the C-apertures with (a) *d*=23.1 nm; the aperture length *a* is obtained by downsizing those values in section 3.2.4 by 1.475

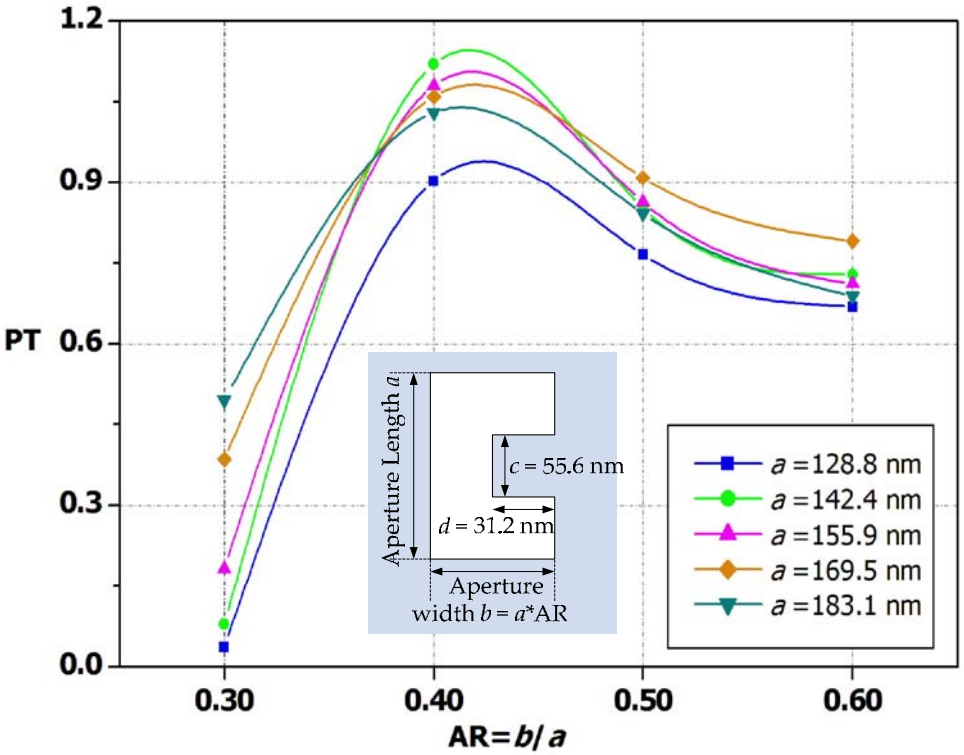

(b)

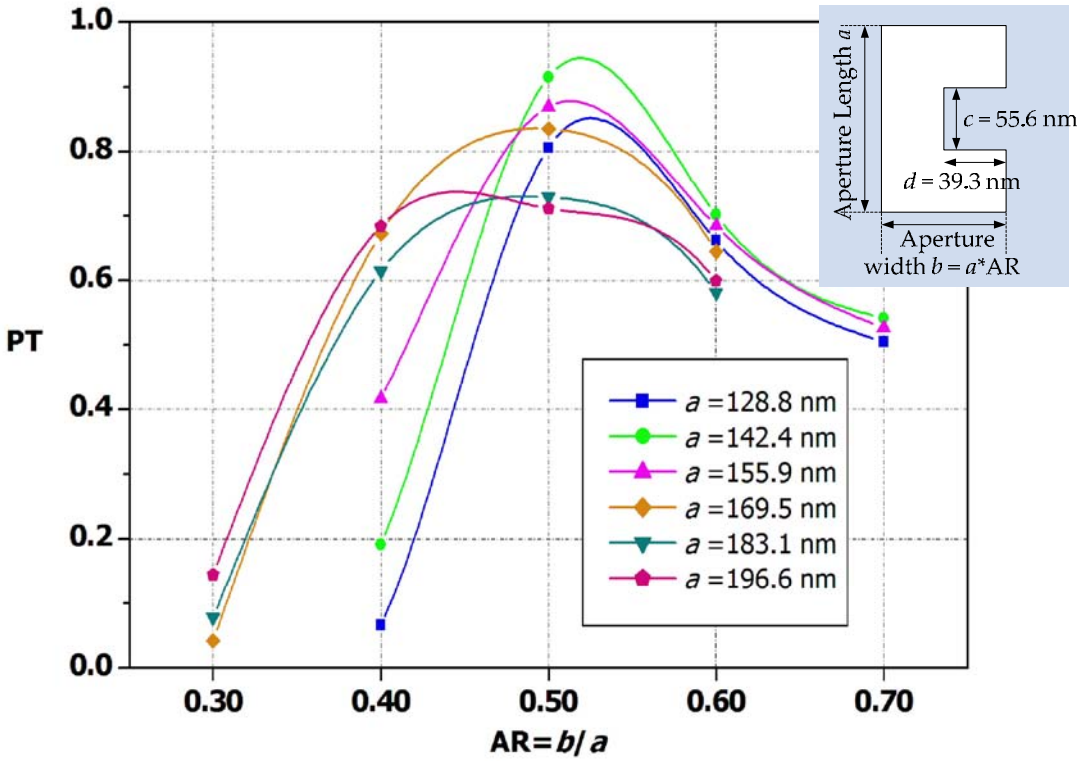

(c)

Fig. 3.3-11 Power throughput of the C-apertures with (b) *d*=31.2 nm and (c) *d*=39.3 nm; the aperture length *a* is obtained by downsizing those values in section 3.2.4 by 1.475

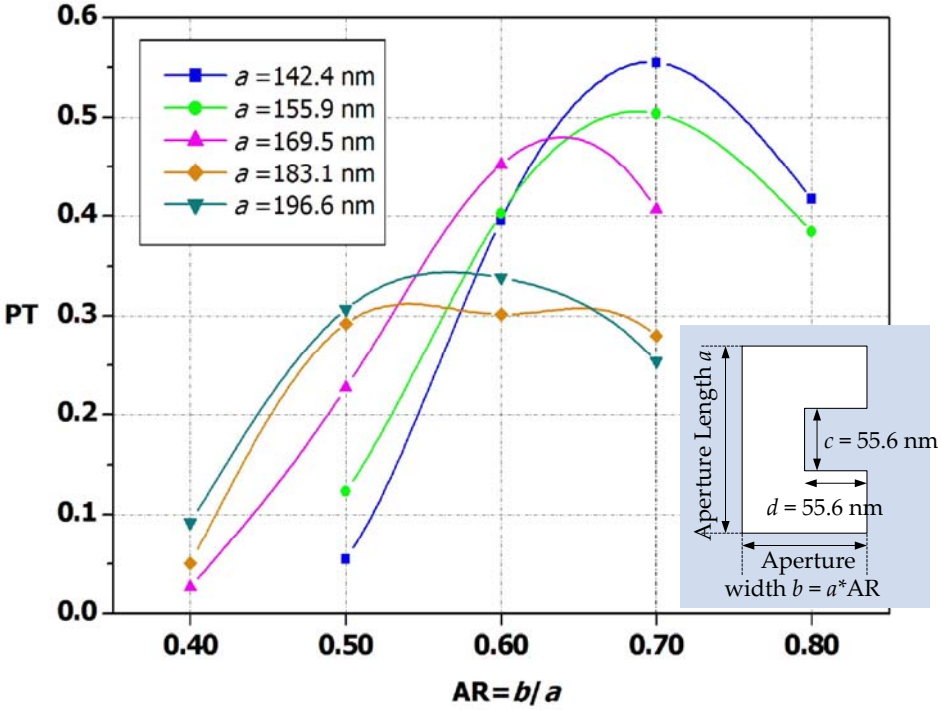

(d)

Fig. 3.3-11 Power throughput of the C-apertures with (d) d=55.6 nm; the aperture length a is obtained by downsizing those values in section 3.2.4 by 1.475

The quantities calculated by

$$\frac{(\text{Gap } g)\times\ (\text{Ridge width } d)}{(\text{Aperture width } b)^2} \quad \text{----(1)}$$

at each peak are particularized in Table 3.3-4. The average is 0.247 with standard deviation of $2.87*10^{-3}$; therefore, the correspondence relation of the integrated case is:

$$\frac{(\text{Gap } g)\times\ (\text{Ridge width } d)}{(\text{Aperture width } b)^2} \cong 0.247$$

Compared to the correspondence relation of the freestanding case, which is:

$$\frac{(\text{Gap } g)\times\ (\text{Ridge width } d)}{(\text{Aperture width } b)^2} \cong 0.247\,,$$

these two average values are almost consistent, meaning the correspondence relation still validates in the integrated case.

Table 3.3-4 The quantities corresponding to each peak in Fig. 3.3-11 computed by eq. (1)

Aperture length a (nm) \ Ridge width d (nm)	**23.1**	**31.2**	**39.3**	**55.6**
128.8	0.247	0.244	0.242	
142.4	0.250	0.249	0.249	0.247
155.9	0.249	0.250	0.250	0.250
169.5	0.246	0.247	0.249	0.249
183.1	0.240	0.243	0.245	0.245
196.6			0.248	0.250
Average	***0.247***			
Standard Deviation	***2.87E-03***			

3.3.6 Comparison (1) – Normal Incidence

The optimum C-aperture in the integrated case is compared with a 60*60 nm^2 square aperture, as shown in Table 3.3-5 and Fig. 3.3-12. Surprisingly, this C-aperture just comes from linearly downsizing the optimum one in the freestanding case.

Compared to a 60*60 nm^2 square aperture, the C-aperture can afford the power throughput enhanced by a factor of 1.28*10^4; additionally, a more circle-like spot is produced due to the reduction in X direction as illustrated by electric field energy density distribution in Fig. 3.3-12. Therefore, an enhancement with 1.67*10^4 in power throughput density is achieved, which can rival the freestanding case. Besides optimizing the C-aperture dimensions, linear downsizing effect and invariance of correspondence relation are the greatest contributions that provide a regulation for design, fabrication and application of the C-aperture.

Table 3.3-5 Comparison between the optimum C-aperture and a 60*60 nm^2 square aperture

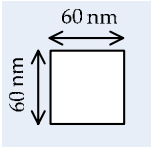

Square	**Aperture type**	**C-shaped**
1.00E-04	**Power throughput**	1.28E+00
147*105	**Spot size (nm*nm)**	108.2*109.3
6.50E-03	**Power throughput density**	1.08E+02

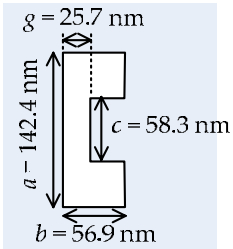

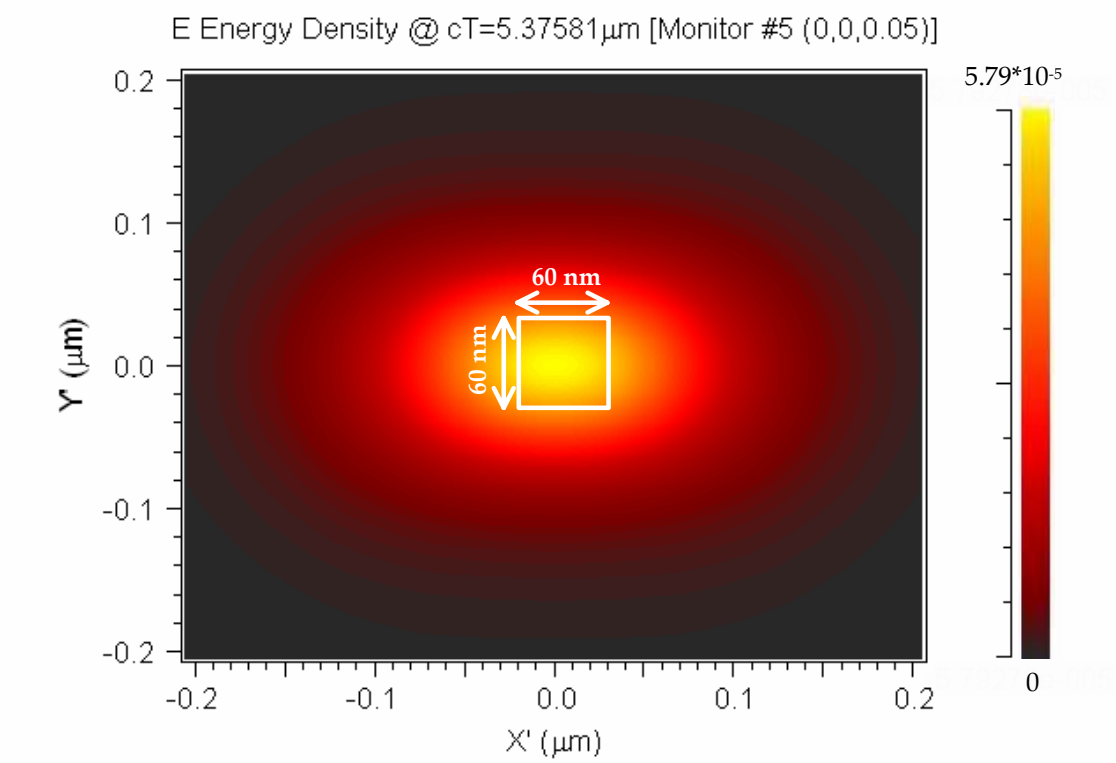

(a)

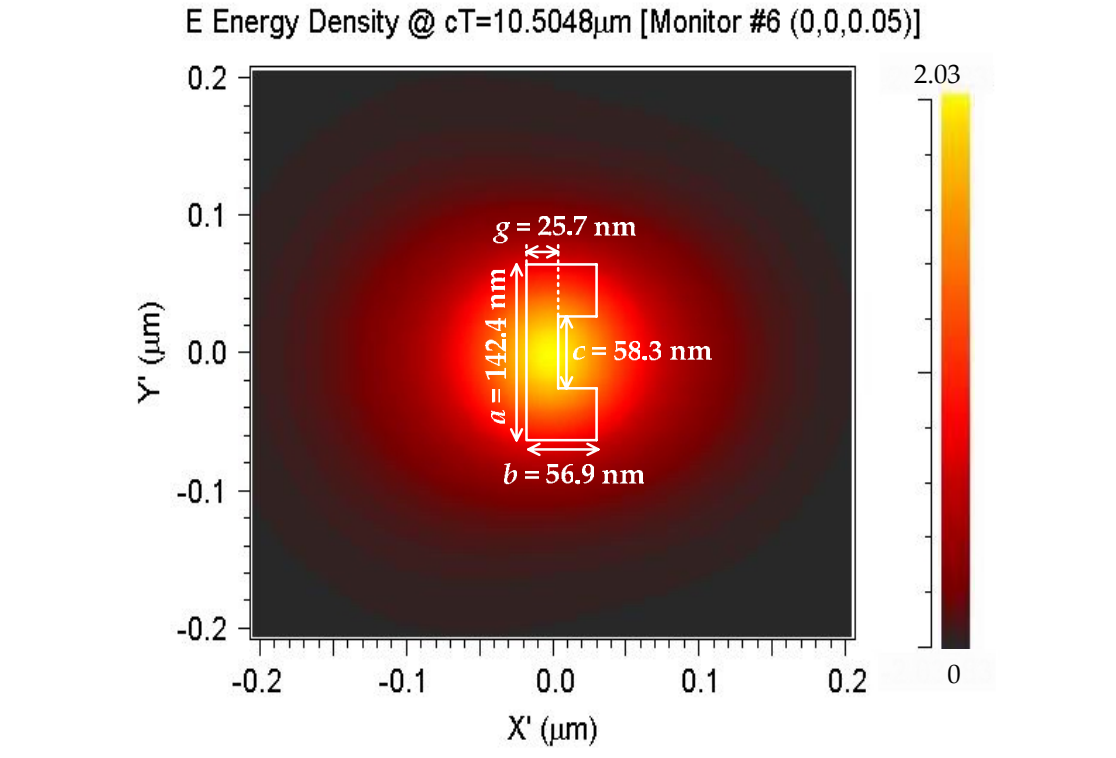

(b)

Fig. 3.3-12 Electric field energy density of (a) a 60*60 nm² square aperture and (b) the C-aperture, the shape and dimensions of the apertures are outlined and labeled.

3.3.7 Oblique Incidence

The further power throughput enhancement in the freestanding case performed by oblique incidence is an impulse to try out if the C-aperture on a slanting end face of the fiber can have better optical performance. The definition of the incident angles, phi (Φ) and theta (θ), are identical to those in the freestanding case; the dimensions of the optimum C-aperture derived from the previous sections are adopted and plotted in Fig. 3.3-13.

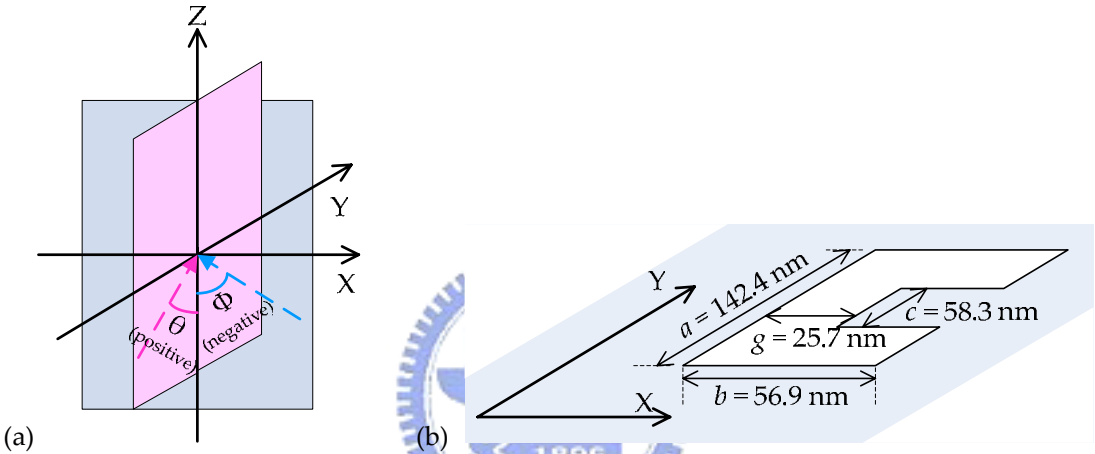

Fig. 3.3-13 (a) Definition of incident angle phi (Φ) and theta (θ) and (b) the C-aperture dimensions

The power throughput as a function of Φ is fitted almost completely by a Gaussian function as well, but the center of the peak moves to -39°, where the power throughput reaches up to 1.9 and is 1.5 times greater than that at normal incidence, as shown in Fig. 3.3-14. Although the center of the peak in the integrated case differs from that in the freestanding case, the extent of enhancement resulted from the oblique incidence is nearly the same. However, the spot size is almost unaffected by incident angle Φ, as listed in Table 3.3-6.

Table 3.3-6 Spot size at different incident angle Φ

Φ	Spot size (nm)	
	X	Y
-45	108.2	108.5
-42	108.2	108.5
-39	105.6	108.5
-36	108.2	108.5
-33	105.6	108.5
-30	105.6	108.5
-27	105.6	108.5
-24	105.6	108.5
-21	105.6	108.5
-18	105.6	108.5
-15	105.6	108.5
-12	105.6	108.5
-9	105.6	108.5
-6	108.2	108.5
-3	108.2	108.5
0	105.6	108.5
3	108.2	108.5
6	108.2	108.5
9	108.2	108.5
12	108.2	108.5
15	108.2	112.8

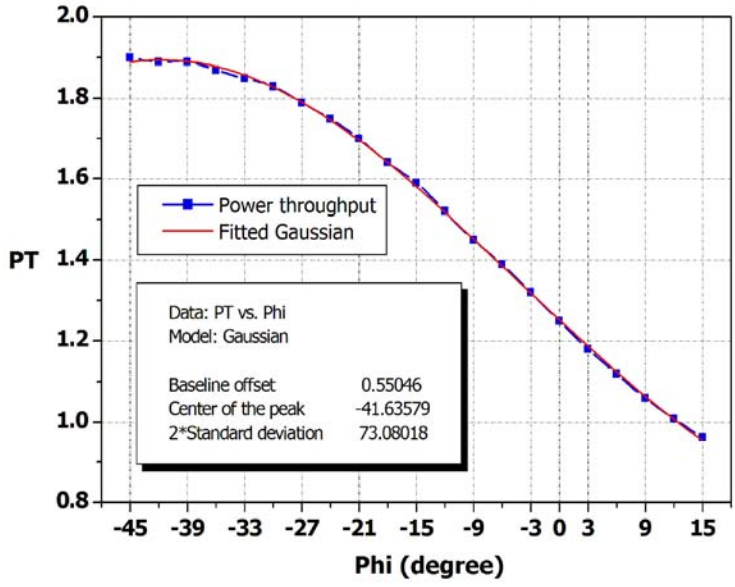

Fig. 3.3-14 Power throughput as a function of incident angle Φ

On the other hand, the effect of θ on the power throughput and the spot size are not very obvious, as shown in Fig. 3.3-15 and Table 3.3-7.

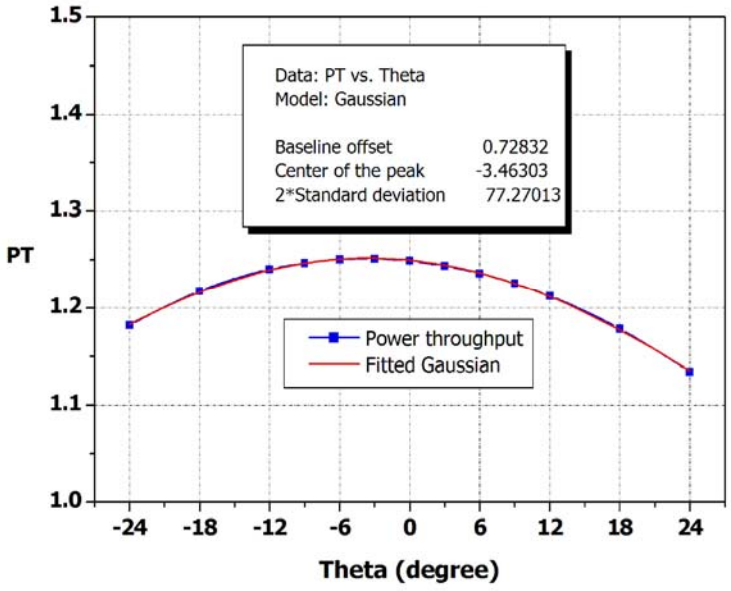

Fig. 3.3-15 Power throughput as a function of incident angle θ

Table 3.3-7 Spot size at different incident angle θ

θ	Spot size (nm)	
	X	Y
-24	108.2	108.5
-18	108.2	108.5
-12	108.2	108.5
-9	108.2	108.5
-6	108.2	108.5
-3	105.6	108.5
0	105.6	108.5
3	105.6	108.5
6	105.6	108.5
9	105.6	108.5
12	105.6	108.5
18	108.2	108.5
24	108.2	108.5

3.3.8 Comparison (2) – Oblique Incidence

According to these simulation results, the C-aperture at oblique incident angle (Φ, θ) of (-39°, 0°) performs the best. Compared to a 60*60 nm^2 square aperture, as displayed in Table 3.3-8, the improvements of this C-aperture are a factor of 1.90*10^4 in power throughput, a much reduced and circle-like spot size and an enhancement with 2.50*10^4 in power throughput density.

Table 3.3-8 Comparison between the optimum C-aperture and a 60*60 nm^2 square aperture

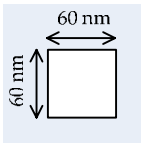

Square	Aperture type	C-shaped
1.00E-04	**Power throughput**	1.90E+00
147*105	**Spot size (nm*nm)**	105.6*108.5
6.50E-03	**Power throughput density**	1.61E+02

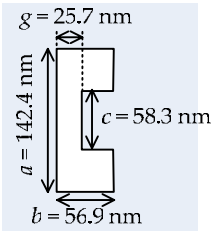

3.4 Summary

With regard to the relation between transmission and the C-aperture dimensions, there are four features that can manifestly characterize C-aperture as a single ridge waveguide:

1. With fixed aperture parts *a* and *b*, gap *g* is a major factor to power throughput and there is a cut-off gap staying invariant regardless of ridge length *c*.

2. Transmission behavior can be reproduced with the C-aperture dimensions normalized to the incident wavelength.

3. Most of the transmitted energy is confined in the area formed by ridge length *c* and gap *g*.

4. The transmitted energy is carried by a propagation wave rather than an evanescent wave.

Furthermore, two important connections between the freestanding and integrated cases are found:

1. Linearly downsizing effect

2. Invariance of the correspondence relation,

which can facilitate designing and fabricating the C-aperture on other dielectric substrates.

Finally, the improvements of the C-aperture superior to a 60*60 nm^2 square aperture are summarized:

For the freestanding case

1. At normal incidence, the optimum C-aperture is a factor of $2.78*10^4$ and $2.80*10^4$ in power throughput and power throughput density respectively at a comparable subwavelength spot size of 117.8*136.4 nm^2.

2. At oblique incident angle (Φ, θ) of (-27°, 0°), the optimum C-aperture is a factor of $4.02*10^4$ and $4.10*10^4$ in power throughput and power throughput density respectively at the same spot as normal incidence.

For the integrated case:

1. At normal incidence, the optimum C-aperture provides enhancements with $1.28*10^4$ and $1.67*10^4$ in power throughput and power throughput density respectively at a more reduced and circle-like subwavelength spot size of 108.2*109.3 nm^2.

2. At oblique incident angle (Φ, θ) of (-39°, 0°), the optimum C-aperture provides enhancements with $1.90*10^4$ and $2.50*10^4$ in power throughput and power throughput density respectively at the same spot as normal incidence.